technische universität
dortmund

Advanced Laboratory Course

Particle Physics

Measurement of matter-antimatter asymmetries with the LHCb experiment

---

Koen Denekamp & Riana Shaba

June 2025

Contents

1 Introduction

1.1 The LHCb detector

The LHCb detector was conceived specifically to perform experiments in flavour physics. According to the design specifications [5], it was created to study CP-violation and other phenomena related to the b quark. CP-violation concerns the problem that there should have been an equal amount of matter and antimatter created at the Big Bang. Matter and antimatter annihilate when they get close together, so there should be no matter in the universe. This is not true, as everything around us is made out of matter.
The LHCb detector, shown in Figure 1, has several components. In this diagram, the protons collide at the left, where $z = 0$, and in the middle, where $y = 0$. The particles created in the collision will thus be detected if they move from left to right. It should be noted that particles are created in every direction, but particles containing b and c quarks mostly move in the positive z or negative z direction. This is the order that will be followed in explaining the different components as well.

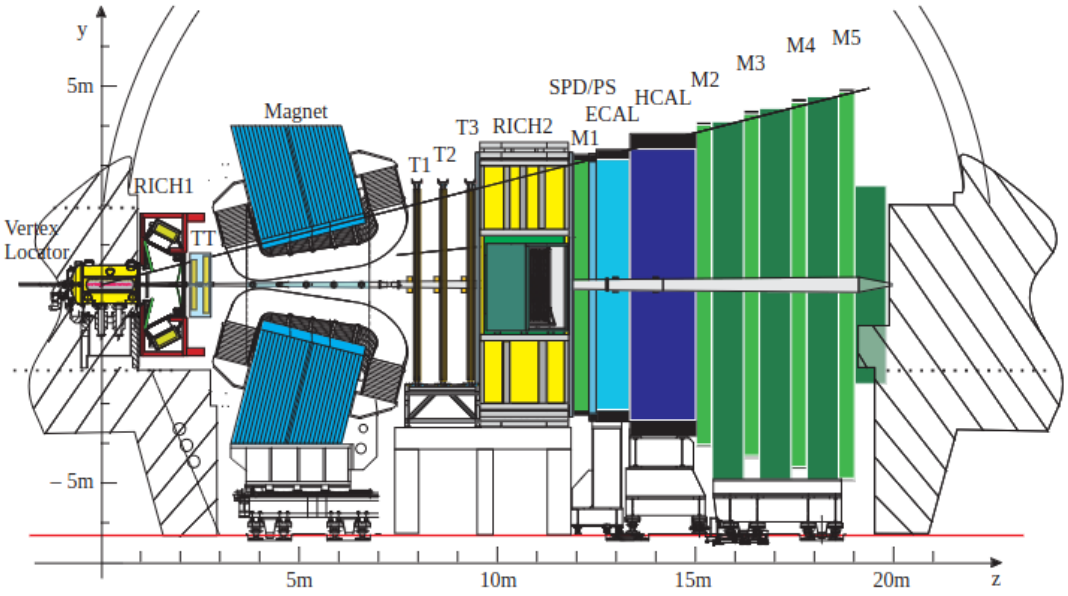

Figure 1: Diagram of the LHCb detector with the separate components. From Ref. [5].

The decaying particles first encounter the Vertex Locator (VELO). This segment is part of the tracking system, as it both reconstructs primary and secondary vertices of particles,

their decays, and the trajectories [4].
During Run 2, the time on which the Monte Carlo simulations that generated the data were based, the particles then entered the Tracker Turicensis (TT).
Then the particles enter the first Ring-Imaging Cherenkov detector (RICH1). This part of the detector is used for particle identification [2]. It works due to the fact that different mediums have a different speed of light: when a particle travels faster than the speed of light in that medium, the particle disrupts the molecules of the medium in such a way that they release photons.
Based on the Cherenkov angle between the track of the particle and the line one can draw across the side of the rings, the velocity of the particle can be determined [3]. This means the angle is related to the velocity.
Since the momentum of the particle is measured using the tracking stations, and the magnet for charged particles [3], it is possible to combine the momentum and velocity measures to find an estimate of the mass of a particle.
Then there is a magnet used to measure whether a particle is positively, negatively, or neutrally charged, as these groups of particles will bend in different directions, or not at all for neutrally charged particles. It is also used to calculate the momentum of charged particles since high-momentum particles bend less than low-momentum particles.
T1, T2, and T3 are tracking stations consisting of two parts. The inner part, known as the Inner Tracker (IT), is close to the beam pipe. The outer part, known as the Outer Tracker (OT) in placed around the IT. The IT and the TT together are also known as the Silicon Tracker [7].
Then another RICH detector is encountered, before entering the SPD/PS layers. SPD stands for Scintillator Pad Detector, while PS stands for PreShower. The goal of the SPD is to identify charged particles and to separate electrons from protons. The PS identifies electromagnetic particles. These steps are taken, since the calorimeters that follow these layers require good background rejection and reasonable efficiency [6].
There are two calorimeters. One specifically for electrons and photons, known as the ECAL and one for hadrons, known as the HCAL. These detectors measure the energy of the incoming particles.
Lastly there are the five muon detector layers, which are also part of the tracking system. Muons pass through the subsystems of the detector, as they have a very low interaction probability.

1.2 Physics

In this analysis we use data taken by the LHCb detector during Run 1 period. It contains $B^{\pm} \to h^{+}h^{-}h^{\pm}$ decays, where $h = \pi$ or $h = K$ [1]. We are interested in comparing the

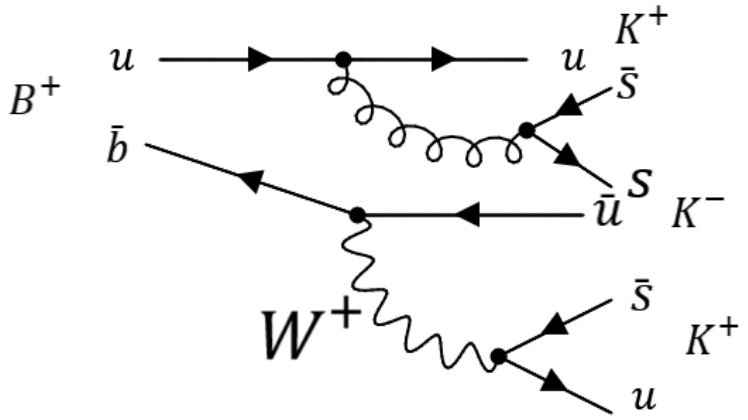

Figure 2: Feynman diagram showing the dominant $B^+ \to K^+K^+K^-$ decay path.

$B^+ \to K^+K^+K^-$ decay rates to its antiparticle, the $B^- \to K^+K^-K^-$ decay rates. In Figure 2, we show the dominant $B^+ \to K^+K^+K^-$ Feynman diagram.
A similar Feynman diagram can be created for the $B^- \to K^+K^-K^-$ decay.
CP violation source is the weak interaction, and it is parameterised by the Cabibbo-Kobayashi-Maskawa (CKM) matrix. The matrix is shown in (1) written in Wolfenstein parameterisation with four parameters and the approximation to order $\mathcal{O}(\lambda^3)$, where $\lambda = \sin(\theta_C) \sim 0.2$ gives the strength of the coupling between different generations. The angle θ_C is the Cabibbo angle, and η is the complex phase which introduces CP violation. The coupling is the strongest for quarks of the same generation, and is weaker for those from the first and second generations, and much weaker for the first and third generations. This is a unitary matrix that entails information about the weak decays of three generations of quarks, as it describes the probability of a flavour *j* down-type quark transitioning to another flavour *i* up-type quark via weak interaction. These transition probabilities are proportional to $|V_{ij}|^2$.

$$V_{\mathrm{CKM}} = \begin{pmatrix} V_{ud} & V_{us} & V_{ub} \\ V_{cd} & V_{cs} & V_{cb} \\ V_{td} & V_{ts} & V_{tb} \end{pmatrix} \simeq \begin{pmatrix} 1-\frac{1}{2}\lambda^2 & \lambda & A\lambda^3(\rho - i\eta) \\ -\lambda & 1-\frac{1}{2}\lambda^2 & A\lambda^2 \\ A\lambda^3(1-\rho-i\eta) & -A\lambda^2 & 1-\frac{1}{2}\lambda^2 \end{pmatrix} \quad (1)$$

We can quantify CP violation by measuring the CP asymmetry A_{CP}, which measures the difference in behaviour of a particle and its CP-conjugate, as below:

$$A_{CP} = \frac{N^+ - N^-}{N^+ + N^-} \quad (2)$$

A difference in the abundances of the two decays we are considering in this laboratory course would be a strong indication for a difference between matter and antimatter, a violation of the Charge Parity symmetry.

2 Data Analysis

2.1 Reconstruction of invariant mass of final state particles

We begin by defining the momentum magnitudes and energies of the three hadrons, according to the following equations:

$$|p|_H = \sqrt{p_x^2 + p_y^2 + p_z^2} \tag{3}$$

$$E_H = \sqrt{|p|_H^2 + m_K^2}, \quad m_K = 493.677\,\text{MeV} \tag{4}$$

We then find the energy of the supposed B meson by summing the three energies:

$$E_B = E_{H_1} + E_{H_2} + E_{H_3}. \tag{5}$$

We calculate the momentum magnitude by summing among the components, like Eq. 5, and then applying Eq. 3. We then find the invariant mass of the mesons according to

$$m_{inv} = \sqrt{E_B^2 + |p|_B^2}. \tag{6}$$

The histogram of the resulting invariant mass distribution can be found in Figure 3. The peak is found at 5279.25 MeV. This corresponds well with known B meson mass values.

In the following, we filter out the data so that it only contains events that have a high probability of containing kaons in the final state, just like the decay channels we are interested in $\mathrm{B}^+ \to \mathrm{K}^+\mathrm{K}^+\mathrm{K}^-$ or its antiparticle equivalent $\mathrm{B}^- \to \mathrm{K}^+\mathrm{K}^-\mathrm{K}^-$. In our data selection, we ensure that the events of three final candidates are not muons, and we require that each candidate has a probability less than 0.5 of being a pion, `H1_ProbPi` < 0.5, and that each candidate has a probability above 0.5 of being a kaon, `H1_ProbK` > 0.5, while requiring the same for the second and the third candidate.
After applying this selection to the data, we plot histograms of the probability distributions of the final state particle being a pion as shown in Figure 4a or a kaon shown in Figure 4b.

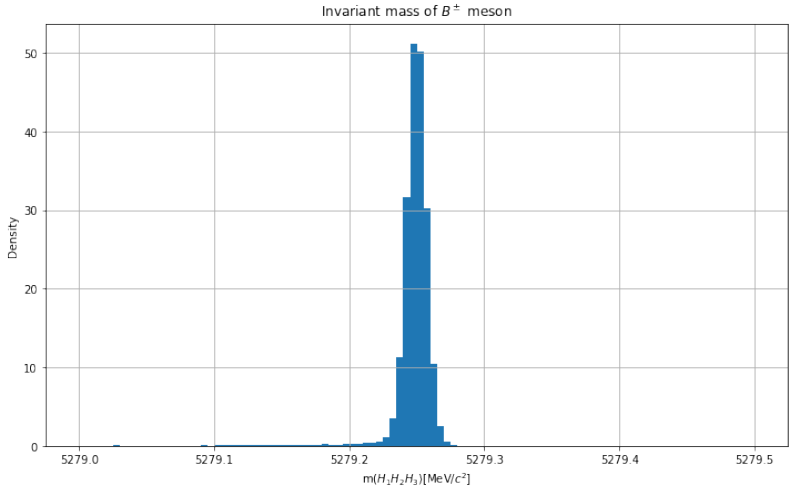

Figure 3: Histogram showing the initial invariant mass distribution of the B meson.

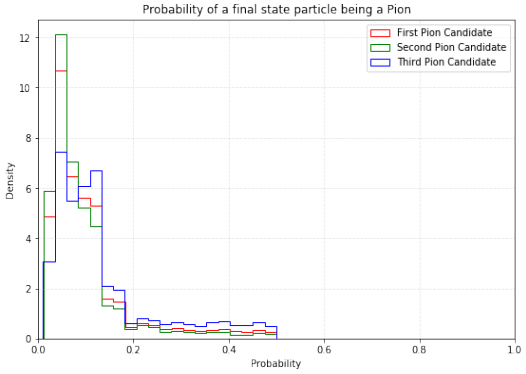

(a) Histogram showing the probability distribution of the final state particle being a pion.

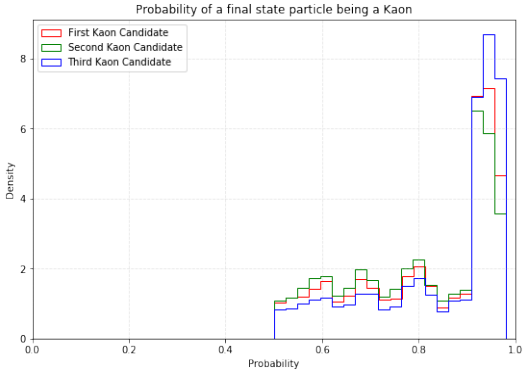

(b) Histogram showing the probability distribution of the final state particle being a kaon.

Figure 4: Histograms showing the probability distribution of the final state particle being a pion or a kaon for the three candidates. The probability cut for pions is less than 0.5 and for kaons is above 0.5.

A 2D image of these probabilities is shown in Figure 5 to indicate how the particle candidates that have a high probability of being a kaon, have a low probability of being a pion.

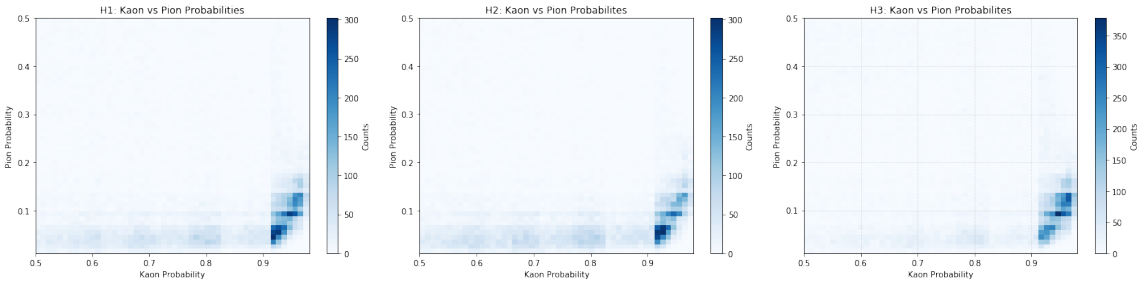

Figure 5: A 2D histogram showing the pion and kaon probabilities for all three candidates. For particles with a high probability of being a kaon, the probability of being a pion is very low.

Then we calculate the invariant mass of the $B^{\pm}$ meson for the real data in the same way as before, and plot the invariant mass distribution in a histogram which is shown in Figure 6a. After looking at this distribution, we selected a cut for the mass, that being $5200\ \mathrm{MeV/c^2} \leq m \leq 5400\ \mathrm{MeV/c^2}$, which approximately contains most of the signal and at the same time removes as much background as possible. The histogram with this mass cut applied is shown in Figure 6b and has a peak at 5287.00 MeV/c^2.

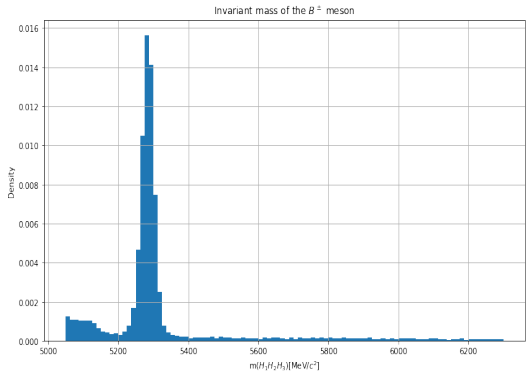

(a) Histogram showing the invariant mass distribution of the $B^{\pm}$ meson.

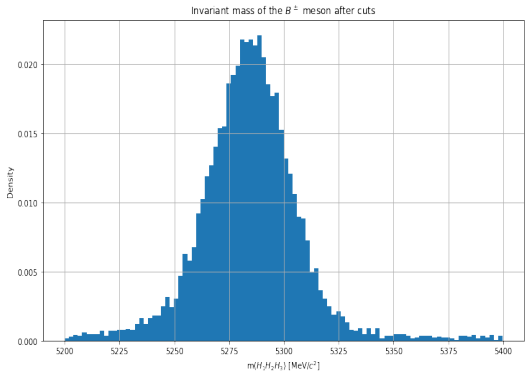

(b) Histogram showing the invariant mass distribution of the $B^{\pm}$ meson after the cut.

Figure 6: Histograms showing the invariant mass distribution of the $B^{\pm}$ meson. The plot on the left has no cuts applied to the mass, while the plot on the right has a mass cut of $5200\ \mathrm{MeV/c^2} \leq m \leq 5400\ \mathrm{MeV/c^2}$ applied so that it contains as much signal and removes as much background as possible. The mass peak is at 5287.00 MeV/c^2.

When comparing these plots with the plots from the simulated data, we see some differences starting with the noticeable background contributions under and around the

peak. The tails on both sides of the peak are not even symmetrical possibly due to detector effects, limitation of resolution and the presence of other physics processes. The simulated data has a peak at 5279.25 MeV/c^2, which is very close to the PDG data, while the peak of invariant mass for the real data is at 5287.00 MeV/c^2.

2.2 The global matter-antimatter CP asymmetry

Further into the analysis, we look at global matter-antimatter differences, meaning that we inspect for differences across all ranges of energy and momentum of kaons in the final state of the $B^{\pm}$ mesons decay. We look at both the B^+ and B^- mesons, and calculate the global CP asymmetry from its definition given in Eq. 2.
We have N^+ = 12390 which is the number of B^+ events, and N^- = 11505 which is the number of B^- events. The statistical uncertainty of the asymmetry is defined as in the following:

$$\sigma_A = \sqrt{\frac{1 - A^2}{N^+ + N^-}} \tag{7}$$

Taking into account only the statistical uncertainty, we estimate a global CP asymmetry of

$$A_{CP} = 0.037 \pm 0.006(\text{stat.})$$

The significance of the result is estimated as the ratio A/σ_A, and we determine it to be 5.729σ.
Since there are other sources of uncertainties, such as systematic uncertainties, we have to take into account such a systematic uncertainty that comes from the expected production asymmetry of the $B^{\pm}$ meson, which is taken as $\sigma_{sys} = 0.010$. We recalculate the total uncertainty by adding up the statistical and systematic uncertainties in quadrature:

$$\sigma = \sqrt{\sigma_A^2 + \sigma_{sys}^2} \tag{8}$$

Hence, the global CP asymmetry is found to be

$$A_{CP} = 0.037 \pm 0.006(\text{stat.}) \pm 0.010(\text{sys.})$$

with a significance of 3.110σ.

2.3 The local matter-antimatter CP asymmetry

We are interested in the direct decay from a B meson to three mesons, but our data also includes decay with intermediate resonances. These must be removed, which we will do

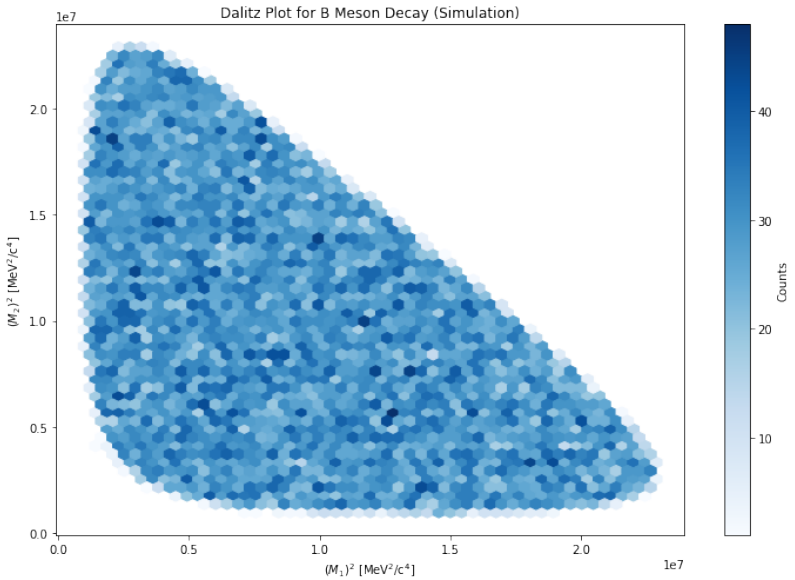

Figure 7: Dalitz plot showing the distribution of masses for simulation data.

through the use of Dalitz plots. Our Dalitz plots are 2D histograms that show the mass squared of the two neutral combinations that can be made from a $K^+K^-K^+$ system. As an example, we should this applied to the simulation data, where there are no intermediate resonances, and we thus see, in Figure 7, a uniform distribution.
If we apply assign a certain combination to subset 1 or 2 randomly, we get poor visibility in the figure. Hence, it is chosen to separate the two subsets based on invariant mass. Of each pair, the combination with the highest invariant mass is sent to one subset, and the combination with the lowest invariant mass is sent to the other. This is shown in Figure 8, where we can see one horizontal and one vertical bar of resonance, representing neutral D mesons and their antiparticle counterpart.
Hence, we remove any events in these bars; we exclude $0.33 \cdot 10^7\ \mathrm{MeV}^2/\mathrm{c}^4 \lesssim (M_{R^0_{\mathrm{low}}})^2 \lesssim 0.36 \cdot 10^7\ \mathrm{MeV}^2/\mathrm{c}^4$ and $1.12 \cdot 10^7\ \mathrm{MeV}^2/\mathrm{c}^4 \lesssim (M_{R^0_{\mathrm{high}}})^2 \lesssim 1.2 \cdot 10^7\ \mathrm{MeV}^2/\mathrm{c}^4$.

After removing the charm quark resonances, we plot 8×8 binned histograms of ordered Dalitz plot to show the number of B^+ and B^- candidates, which is determined in each bin as shown in Figure 9a and Figure 9b.

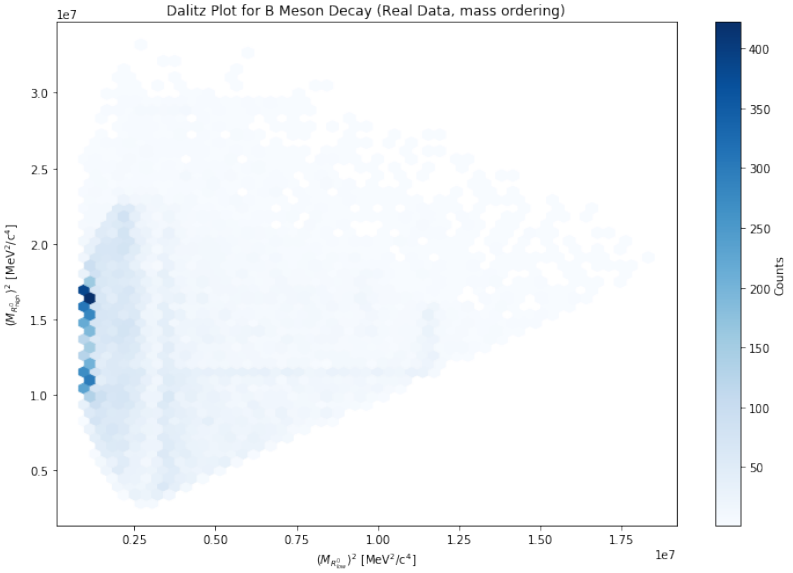

Figure 8: Dalitz plot showing the distribution of ordered masses for real data.

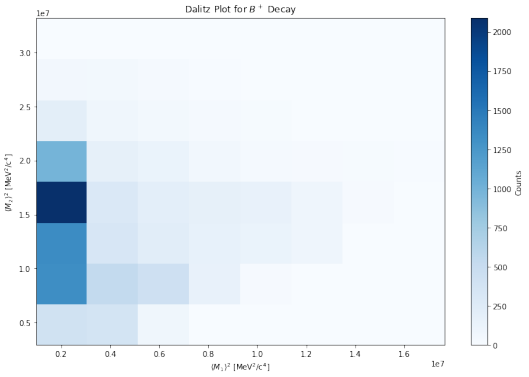

(a) Binned histogram of the ordered Dalitz plot for B^+ decay.

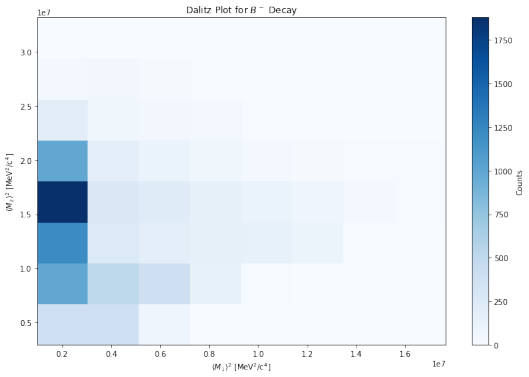

(b) Binned histogram of the ordered Dalitz plot for B^- decay.

Figure 9: Binned histograms of the ordered Dalitz plots for the B^+ and B^- decay candidates.

The local CP asymmetry is calculated between each bin of the B^+ and B^- Dalitz plots as shown in Figure 10a. We observe bins that have significant positive or negative asymmetry, and other bins showing CP violation of different sizes. The significance of the asymmetry in each bin with the systematic uncertainty coming from the expected

production asymmetry taken into account is shown in Figure 10b.

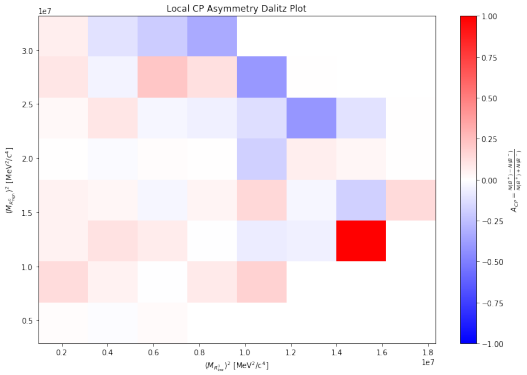

(a) The local CP asymmetry calculated in each bin of the Dalitz plots. The colorbar shows the variation of asymmetry values from the highest (1 and -1) to lowest (0).

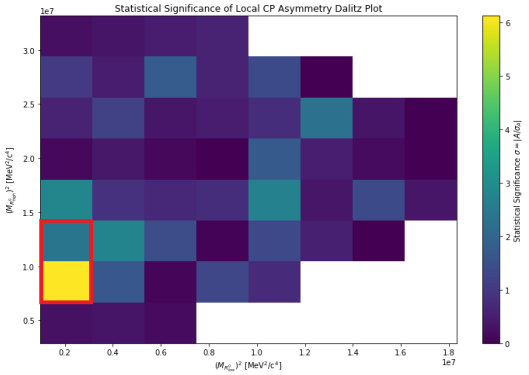

(b) The significance calculated in each bin of the Dalitz plots. The area marked with red is chosen for investigating the local CP asymmetry.

Figure 10: The local CP asymmetry and the significance of the asymmetry calculated between each bin of the B^+ and B^- Dalitz plots after the removal of charm resonances. In the asymmetry plot, the colorbar shows the variation of asymmetry, where red and blue bars have relatively the most asymmetry, while brighter bars do not. In the significance plot, the area enclosed in red is chosen for investigating the CP asymmetry because of the statistical significance there.

We identified a region of continuous bins with a significance of more than 2σ for investigating the local CP violation, which is marked in red. These bins correspond to this kinematic region:

$$0.10 \cdot 10^7\,\mathrm{MeV}^2/\mathrm{c}^4 \lesssim (\mathrm{M}_{\mathrm{R}^0_{\mathrm{low}}}) \lesssim 0.30 \cdot 10^7\,\mathrm{MeV}^2/\mathrm{c}^4$$

$$0.67 \cdot 10^7\,\mathrm{MeV}^2/\mathrm{c}^4 \lesssim (\mathrm{M}_{\mathrm{R}^0_{\mathrm{high}}}) \lesssim 1.33 \cdot 10^7\,\mathrm{MeV}^2/\mathrm{c}^4$$

For this kinematic region, the local CP asymmetry when taking into account the production asymmetry is found to be:

$$A_{CP} = 0.080 \pm 0.011(\mathrm{stat.}) \pm 0.010(\mathrm{sys.})$$

with a significance of 5.273σ.

Then we use this kinematic region in our data and reconstruct again the invariant mass of B^+ and B^- mesons shown in Figure 11.

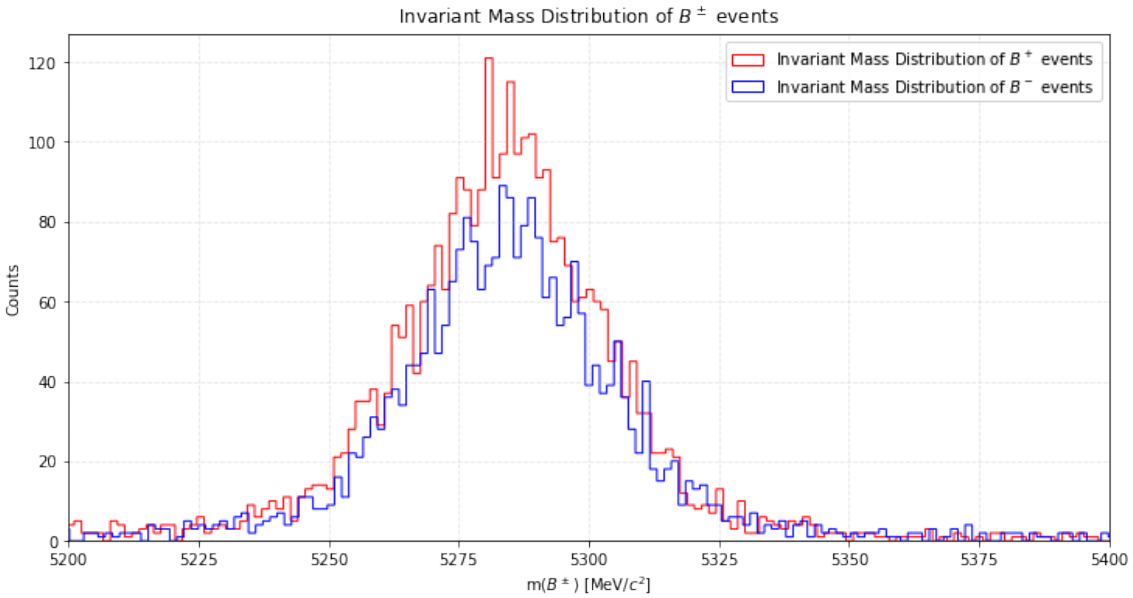

Figure 11: Histogram showing the invariant mass distributions for B^+ and B^- mesons events in the kinematic region of interest where we investigated local CP asymmetry.

3 Conclusions

In this laboratory course, we have performed an analysis of CP violation.
We started by reconstructing the B mesons. We then created cuts to remove as many decays that did not contain three kaons as possible. At this point, the global CP asymmetry was found to be $A_{CP} = 0.037 \pm 0.006(\text{stat.}) \pm 0.010(\text{sys.})$, with a significance of 3.110σ. Then, through the use of Dalitz plots, intermediate charm resonances were removed, as we are interested in the direct decay. Then a region with high CP asymmetry significance was chosen, and the significance of the local CP asymmetry was found to be $A_{CP} = 0.080 \pm 0.011(\text{stat.}) \pm 0.010(\text{sys.})$, with a significance of 5.273σ.
This means we found a statistically significant CP difference between the three Kaon decay modes of B^+ and B^- mesons, at the level of a discovery.

References

[1] AG Albrecht. "Measurement of matter-antimatter asymmetries with the LHCb experiment". In: (April 14, 2022).

[2] N H Brook et al. *LHCb RICH 1 Engineering Design Review Report*. en. Aug. 2004. URL: https://cds.cern.ch/record/897981/files/lhcb-2004-121.pdf.

[3] LHCb collaboration et al. "LHCb Detector Performance". en. In: *International Journal of Modern Physics A* 30.07 (Mar. 2015). arXiv:1412.6352 [hep-ex], p. 1530022. ISSN: 0217-751X, 1793-656X. DOI: 10.1142/S0217751X15300227. URL: http://arxiv.org/abs/1412.6352 (visited on 04/16/2024).

[4] P. Kopciewicz, S. Maccolini, and T. Szumlak. "The LHCb vertex locator upgrade — the detector calibration overview". en. In: *Journal of Instrumentation* 17.01 (Jan. 2022), p. C01046. ISSN: 1748-0221. DOI: 10.1088/1748-0221/17/01/C01046. URL: https://iopscience.iop.org/article/10.1088/1748-0221/17/01/C01046 (visited on 11/20/2023).

[5] LHCb Collaboration. "LHCb reoptimized detector design and performance : Technical Design Report". In: *CERN-LHCC-2003-030*. Technical Design Report (July 2003). http://cds.cern.ch/record/630827.

[6] Eduardo Picatoste Olloqui. "LHCb Preshower(PS) and Scintillating Pad Detector (SPD): commissioning, calibration, and monitoring". In: *J. Phys.: Conf. Ser.* 160 (2009), p. 012046. DOI: 10.1088/1742-6596/160/1/012046. URL: https://cds.cern.ch/record/1293075 (visited on 11/20/2023).

[7] J. van Tilburg. "Tracking performance in LHCb". en. In: *The European Physical Journal C - Particles and Fields* 34.1 (July 2004), s397–s401. ISSN: 1434-6052. DOI: 10.1140/epjcd/s2004-04-041-7. URL: https://doi.org/10.1140/epjcd/s2004-04-041-7 (visited on 04/09/2024).